In situ neutron powder diffraction of Li_6C_{60} for hydrogen storage

Mattia Gaboardi,[1] Samuel Duyker,[2,3] Chiara Milanese,[4] Giacomo Magnani,[1] Vanessa K. Peterson,[2] Daniele Pontiroli,[1] Neeraj Sharma,[5] Mauro Riccò.[1*]

1. *Department of Physics and Earth Sciences, University of Parma, 43124 Parma, Italy.*
2. *Australian Nuclear Science and Technology Organisation, Locked Bag 2001, Kirrawee DC, New South Wales 2232, Australia.*
3. *School of Chemistry, The University of Sydney, Sydney, Australia.*
4. *H2-Lab, Department of Chemistry, University of Pavia, 27100 Pavia, Italy.*
5. *School of Chemistry, University of New South Wales (UNSW), Sydney, Australia.*

** mauro.ricco@fis.unipr.it*

Li_6C_{60} is so far the best performing fullerene-based hydrogen storage material. The mechanism of its reversible hydrogen absorption is not, however, totally known. Here we report the thermal evolution of Li_6C_{60} upon deuterium absorption up to 330 °C and under 60 bar deuterium gas using *in situ* high-intensity neutron powder-diffraction. The good temporal resolution of the data allowed the hydrogenation of Li_6C_{60} and the segregation of lithium hydride (here LiD) processes to be distinguished from a mechanistic point of view. During absorption, Li_6C_{60} undergoes several phase transitions, involving the partial segregation of Li in form of hydride and the expansion of the face-centered cubic (*fcc*) lattice followed by a body-centered cubic (*bcc*) rearrangement of the deuterated fullerenes. The amount of absorbed deuterium was determined by the analysis of the variation in the scattered neutron intensity and confirmed by an *ex situ* desorption measurement. This analysis clarifies the complex physico-chemical reactions behind the absorption mechanism of this model material and highlights the importance of intercalated lithium in triggering the hydrogenation process.

1. Introduction

The first evidence of catalytic hydrogen absorption in fullerides was found in Li_6C_{60} by Teprovich *et al.* in 2012.[1] The hydrogen storage performance of this system was improved by addition of transition metals that increased the hydrogen uptake capacity from 5 to 5.9 wt%.[2] Li_6C_{60} belongs to the alkali-cluster intercalated fulleride family, including materials such as Na_6C_{60},[3] $Li_{12}C_{60}$,[4] and $Na_{10}C_{60}$.[5] In these crystals, the large octahedral or tetrahedral voids of the face-centered cubic (*fcc*) C_{60} structure are occupied by small alkali-metal clusters. These clusters are partly ionized and donate electrons on the C_{60} t_{1u} lowest unoccupied molecular orbital (LUMO).

Muon spin relaxation was recently adopted to study the initial stages of the hydrogenation mechanism in these compounds, in particular for Li_6C_{60}, $Na_{10}C_{60}$, and $Li_{12}C_{60}$.[6,7] In these fullerides, muons showed that the presence of intercalated alkali-metal clusters plays an important role in the dissociation of the hydrogen molecule at moderate temperature, while the highly-charged anionic state of C_{60} readily captures the atomic hydrogen. This process is even more efficient below room temperature.[6] Although the *in situ* thermal evolution of related fullerides, such as $Na_{10}C_{60}$ and $Li_{12}C_{60}$, were investigated by means of *in situ* high-resolution neutron powder-diffraction,[88–10] the study of the Li_6C_{60} system has been largely ignored using this technique or any other detailed structural analysis. Therefore, there is a need to understand the hydrogenation process of Li_6C_{60} from a structural perspective and the combination of deuterium absorption and *in situ* neutron powder diffraction are ideal tools for such analysis.

Essentially, the interplay between the different interactions possible in the system, *e.g.* chemical reactions between C_{60} and hydrogen, reaction between lithium and fullerene and generation of new phases, are mostly the reason behind the observed absorption/desorption profiles exhibited by these materials.

In this paper, we investigate the deuterium absorption by Li_6C_{60} *in situ*, by analysing the thermal evolution of neutron powder-diffraction patterns. Thanks to the high neutron flux and modern

instrumentation, data with a high time-resolution were obtained, necessary to follow the complex absorption pathway of this material.

2. Experimental methods

As different to previous preparation methods, in order to obtain the fully intercalated structure, the use of solvents and LiH were avoided. Li_6C_{60} was synthesized directly from C_{60} powder (MER Corp., 99.99%) by adding stoichiometric amounts of LiN_3 (anhydrified and purified from a 20 wt% solution in H_2O from Sigma-Aldrich) in a mortar and annealing the pellets. Since LiN_3 liquefies at 115 °C before decomposing, Li can be easily intercalated into the C_{60} lattice. The pellets were placed in a closed tantalum cylinder inside a quartz vial connected through a valve to a high-vacuum system. The temperature was raised to 120 °C at 60 °C/h, then to 180 °C at 5 °C/h, then to 240 °C at 20 °C/h, and finally to 350 °C at 60 °C/h. The sample was annealed at this temperature for 20 h and then cooled to room temperature. Neutron powder-diffraction measurements were carried out on the high-intensity neutron powder diffractometer WOMBAT[11] at ANSTO (Sydney, Australia) using an incident neutron wavelength of 2.95825(5) Å, determined using the $La^{11}B_6$ NIST standard reference material 660b. 767 mg of Li_6C_{60} was loaded inside a He glove-box into a pressure-rated stainless steel sample cell of ~8 mm inner diameter and 0.51 mm wall thickness equipped with a gas delivery tube and isolation valve. The sample was positioned on the diffractometer inside an infra-red lamp-type vacuum furnace. The temperature was controlled via a K-type thermocouple at the base of the sample cell, with a second thermocouple attached to the cell above the sample level for monitoring the thermal gradients. The gas line and sample space were evacuated before D_2 was introduced to the sample and maintained at 60 bar using a Hiden Isochema IMI gas-delivery system. 2 min diffraction patterns were collected continuously throughout the experiment, during which the temperature was increased from 40 to 330 °C in steps of 10–20 °C and held at each step for ~ 20 min. The temperature was then held at 330 °C for about 9 h. The

diffraction data were normalized with respect to the incident neutron flux measured by a beam monitor positioned upstream of the sample. An additional set of temperature-dependent data were collected for a nominally-identical sample cell pressurized with 60 bar helium gas. In addition to the intense reflections from the stainless steel cell, some spurious weak peaks were observed, attributed to secondary off-axis scattering from parts of the surrounding sample environment. The scattering from the sample cell and sample environment was taken into account when calculating the total neutron intensity attributed to the sample alone, which was then used to estimate the deuterium content of the sample. The total intensity from the sample was obtained by subtracting from the total neutron counts the total counts obtained from the empty cell, whose temperature-dependent value was fitted by a polynomial function. The deuterium desorption was carried out *ex situ* by heating the sample at 5 °C/min from room temperature up to 390 °C under a hydrogen pressure of 0.5 bar in a PCTPro-2000 manometric instrument by HyEnergy-Setaram.

3. Results

The neutron powder-diffraction pattern of the pristine Li_6C_{60} sample is displayed in Figure 1, showing additional reflections from the stainless steel cell. Unfortunately, it is not possible to simply subtract the empty cell data from the data acquired for the sample in the cell due to differences between the experimental setup that include differences between the cells used and their positioning on the instrument as well as temperature differences. The empty cell diffraction pattern is also shown in Figure 1. The *fcc* lattice of C_{60} (fullerite) may hold in principle only 3 atoms with full occupancy (one in the central octahedral void and two in the tetrahedral ones). If the intercalated ion is sufficiently small (*e.g.* Na or Li),[3–5,12] it is possible to maintain the *fcc* structure by forming small alkali-metal clusters centered in the octahedral or tetrahedral voids of the structure, as happens for Na_6C_{60}, $Na_{10}C_{60}$ and $Li_{12}C_{60}$.[3–5,7] Also Li_6C_{60} is isostructural to C_{60}, exhibiting an *fcc* structure at room temperature. Different from other systems, it contains a minor

fraction of polymeric Li_4C_{60} (below 5%),[13] irrespective of the synthesis procedure. Its structure is similar to the high-temperature monomer phase of Li_4C_{60}, which has a Li cluster in the central octahedral void.[12] Le Bail analysis of the neutron diffraction data shown in Figure 1 gives a lattice parameter for the *fcc* phase of a = 13.815(6) Å. This is slightly lower than the value reported in the literature for Li_6C_{60}, measured using laboratory X-ray powder diffraction.[1] The lattice parameter is also lower than the 14.16 Å of fullerite[14] and this is expected due to the coulombic interaction between Li cations and C_{60} anions, contracting the overall lattice. The structure appears to be a slightly distorted *fcc* lattice, similar to that observed for $Li_{12}C_{60}$.[4] An amorphous fraction is also commonly present in fullerides, characterized by a background below the Bragg peaks.

The collection of neutron-diffraction data in the relevant scattering angle (2θ) 17–80° for the experiment are shown as a function of deuterium pressure and temperature in a two-dimensional plot in Figure 2. The complexity of the experiment and reflections from the stainless-steel cell meant that Le Bail analysis or single peak fitting routines had to be used to extract information from these data. The Li_6C_{60} *fcc* phase above considered for the *in situ* data exhibits the three most intense peaks at scattering angles (2θ) of 21, 35 and 40.5° (the 111, 220, and 311 reflections, respectively). The Li_6C_{60} *fcc* 111 reflection in particular was targeted to follow the evolution of the *a* lattice parameter as a function of temperature. Single peak fitting using a Gaussian function plus a flat background was performed near the peak and the result is shown in Figure 3 and Figure *4*. Up to about 125 °C, the Li_6C_{60} *fcc* 111 and 220 reflections shift to the right as the lattice contracts, while the normalized total counts slightly decrease. This is tentatively attributed to the re-crystallization of the amorphous phase into the *fcc* phase, involving partial Li intercalation, whose ionic character affects the lattice constant. Another hypothesis is that a C_{60} valence-state transition occurs in this temperature range. In fact, the lithium cluster is partly ionized and its valence state could vary with temperature. Such behavior was previously observed in $Li_{12}C_{60}$, where the Li cluster undergoes a geometrical rearrangement close to 250 K.[7] Moreover, a similar lattice collapse was also detected in

$Sm_{2.75}C_{60}$, where negative thermal expansion occurred as a result of a quasi-continuous valence change of Sm ions.[15] Unfortunately, it is not possible to understand the exact origin of this contraction since neutron diffraction data are unable to conclusively support these hypotheses.

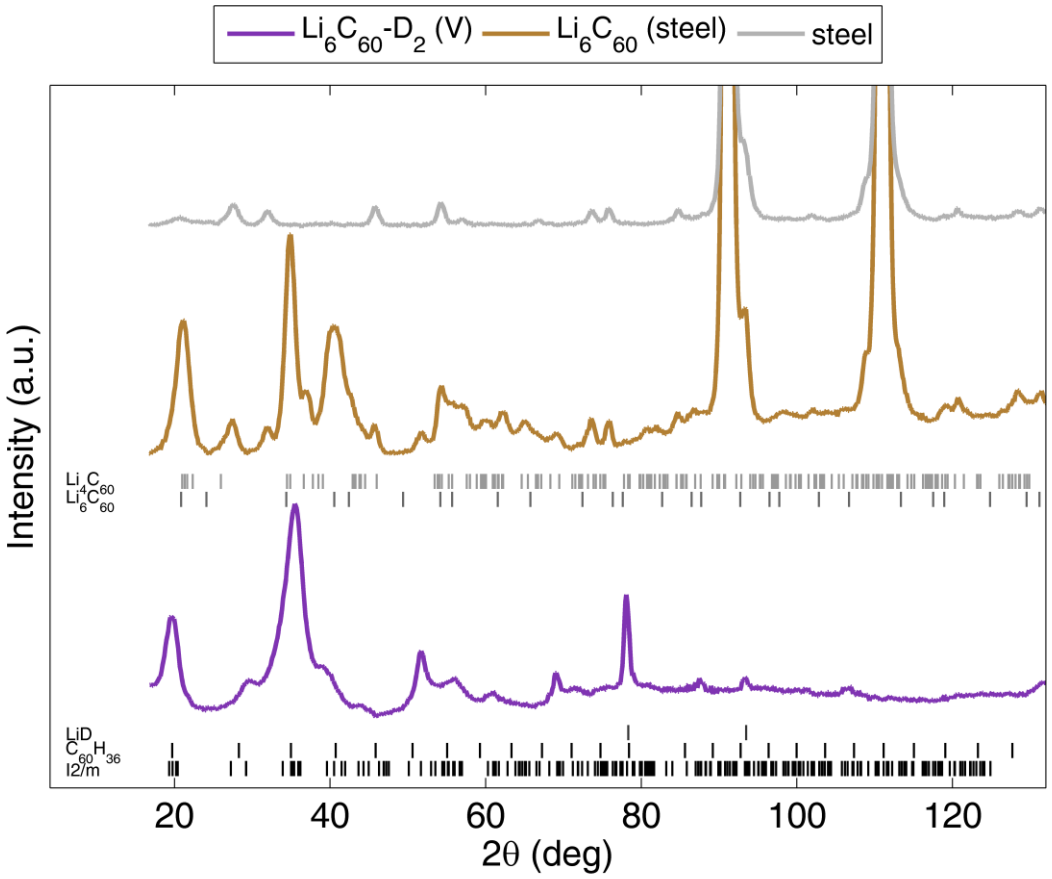

Figure 1: Neutron powder-diffraction patterns of the Li_6C_{60} sample before and after *in situ* deuteration, as measured at room temperature. Patterns from an empty stainless steel cell and deuterated Li_6C_{60} extracted from the cell and placed in a vanadium can are also shown. Vertical bars at the bottom are reflection markers for different phases or space groups

Above 125 °C the data reveal at least three main processes occurring. 1 – Hydrogenation of the C_{60} molecule starting between 130 and 140 °C, when the Li_6C_{60} *fcc* 111 and 220 reflections deviate from their expected thermal evolution and the lattice expands significantly. A similar behavior was

observed in $Na_{10}C_{60}$, where an anomalous lattice expansion was detected between 150 and 250 °C, ascribed to the formation of C-D groups on C_{60} which are responsible for the sudden volume increase.[8] During this expansion, the background increases (as expected for the increasing deuterium content, which is a significant incoherent neutron scatterer) and the intensities of the Li_6C_{60} *fcc* 111 and 220 reflections decrease. This phase transition is a slow process and ends at about 300 °C, when the lattice expansion rate slows down. 2 – A process involving a new reflection, where during the expansion around 200 °C a peak appears at $2\theta = 77.3°$, believed to be the cubic LiD 111 reflection.[16] The intensity of this peak increases with temperature up to 305 °C. The LiD 220 reflection is also observed when the sample was removed from the stainless steel cell and measured in a vanadium cell (see Figure 1). 3 – A dramatic structural change above 315 °C and up to the maximum achievable temperature of 330 °C. Here, the integrated intensity of the LiD 111 reflection decreases by about 60% and, at the same time, a new peak at ~35.1° appears. Tentative indexing allowed the latter to be ascribed to the *bcc* hydrofullerene 311 reflection. After reaching the maximum temperature, the Li_6C_{60} *fcc* 220 reflection progressively decreases in intensity and completely disappears after about 4 h at 330 °C. Conversely, the Li_6C_{60} *bcc* 311 reflection increases in intensity and reaches its maximum value after the Li_6C_{60} *fcc* 220 reflection disappears. Despite these changes, the peak at 19.5°, which was previously attributed to the Li_6C_{60} *fcc* 111 reflection, maintains an approximately constant 2θ position during the 330 °C temperature hold. The integrated intensity slightly increases during the first few minutes of the dwell after the phase transition, and then decreases (see Figure 3, region (3)). This is because the Li_6C_{60} *fcc* reflection on the (111) planes and the Li_6C_{60} *bcc* 110 reflection overlap. The fit of this peak is displayed as a function of time and temperature in Figure 4a and b, respectively.

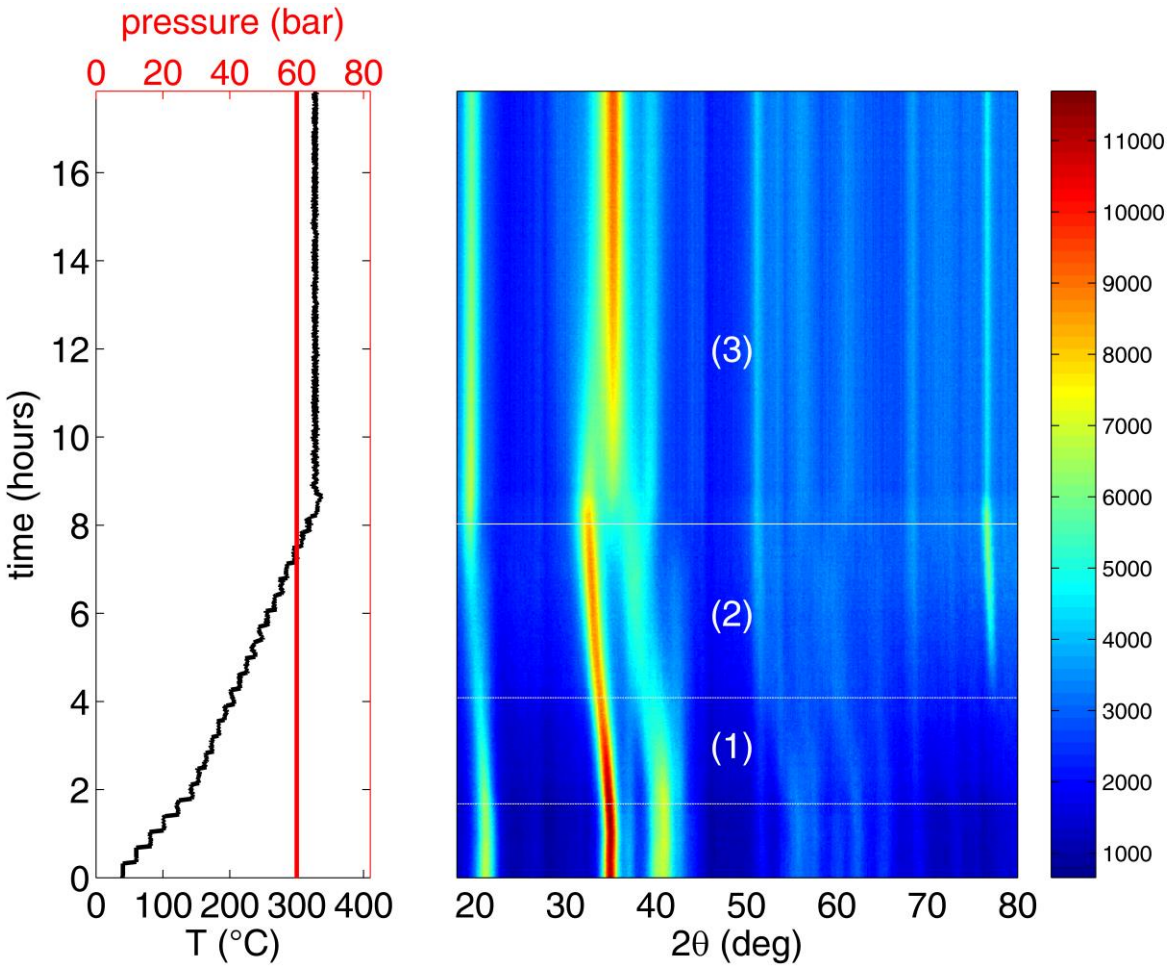

Figure 2: Two-dimensional representation of the time-resolved *in situ* neutron-powder diffraction patterns of Li_6C_{60} in the region between 18 and 80° (right) and the corresponding temperature and D_2 pressure (left). Some weak invariant peaks can be seen that originate from spurious scattering from the sample environment, as shown in Figure 1. The numbers 1, 2 and 3 label the three main transformations discussed in the text.

The cubic lattice parameter calculated from this peak position is shown in Figure 4c, together with the normalized total counts of the sample. The *fcc* lattice parameter increases from ~13.8 to 15.0 Å and the lattice then evolves toward the new *bcc* phase, for which the cubic parameter is ~12.23 Å. The sample's normalized total counts increase from 0.75 to 1 (about 33%) during the *in situ* experiment and this can be correlated to the D_2 content, which would correspond to 3.93 wt% D_2 absorption. An evaluation of the lattice of deuterated compound was carried out by measuring

neutron diffraction data of the sample at the end of the experiment in a vanadium cell at room temperature. Le Bail analysis reveals $Im\bar{3}m$ symmetry with a lattice parameter of 11.816(4) Å (close to what is found for $C_{60}H_{36}$).[17] The lattice parameter value extracted from the Gaussian fitting of the Li_6C_{60} *bcc* 110 reflection ranged from 12.23 to 12.12 Å during the transition at 330 °C in the stainless steel cell (see Figure 4c).

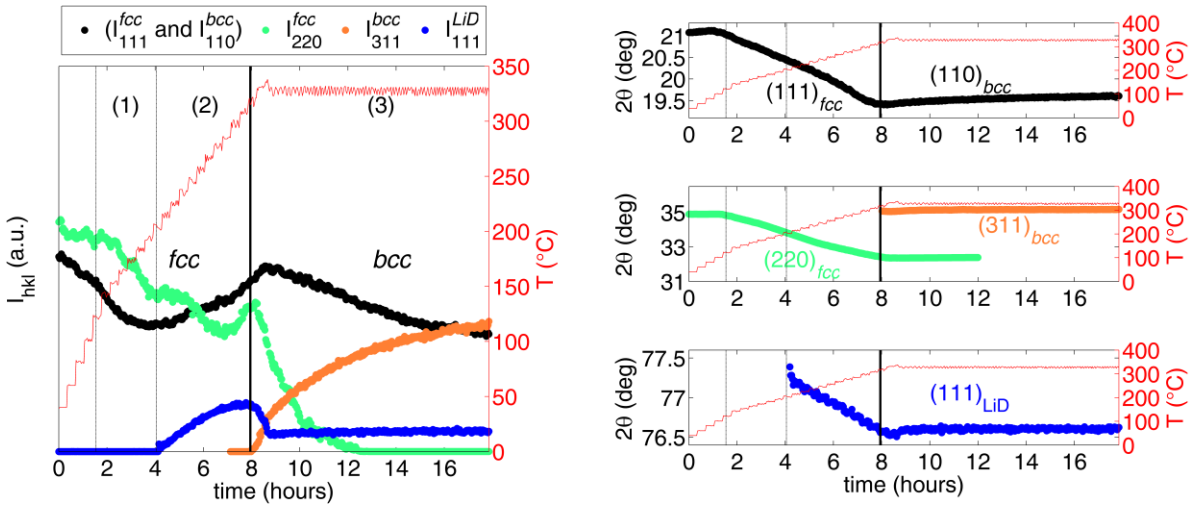

Figure 3: Integrated intensity (left) and 2θ position (right) of selected peaks of the *in situ* data including reflections from Li_6C_{60} (black, green, and orange), and the LiD 111 reflection (blue). The temperature is shown on the right y-axes. The vertical lines mark the main phase changes. In particular, the thicker black vertical line highlights the point at which the *fcc* structure starts to evolve toward the *bcc* phase. The numbers 1, 2 and 3 label the three main transformations discussed in the text.

It is worth noting that the assignment of a *bcc* symmetry to the hydrofulleride $Li_6C_{60}D_y$ lattice should be considered only as an approximation. In fact, while the *bcc* structure indexes well the collected data at low angles, it does not perfectly fit the data at high angles. A more reliable fit was obtained to the data of the sample in the vanadium cell at room temperature with a monoclinic cell with *I*2/*m* symmetry and lattice parameters a = 11.602(3), b = 11.624(2) Å, c = 12.390(1) Å and β = 87.43(1)°. Therefore, the lattice can be assumed as pseudo-*bcc* and the *bcc* case discussed

approximates reasonably well the monoclinic cell. It should also be noted that the Li_6C_{60} sample did not absorb the maximum amount of deuterium, corresponding to the 5 wt% H_2 achieved by treating the sample at 350 °C and 100 bar H_2,[1,6] due to the pressure and temperature limits of the sample environment, but on the basis of a preliminary structural analysis of the fully hydrogenated phase, no dramatic changes in the structure are expected during the increase from 2 to 5 wt% hydrogen, apart from an expected small increase in lattice parameter.

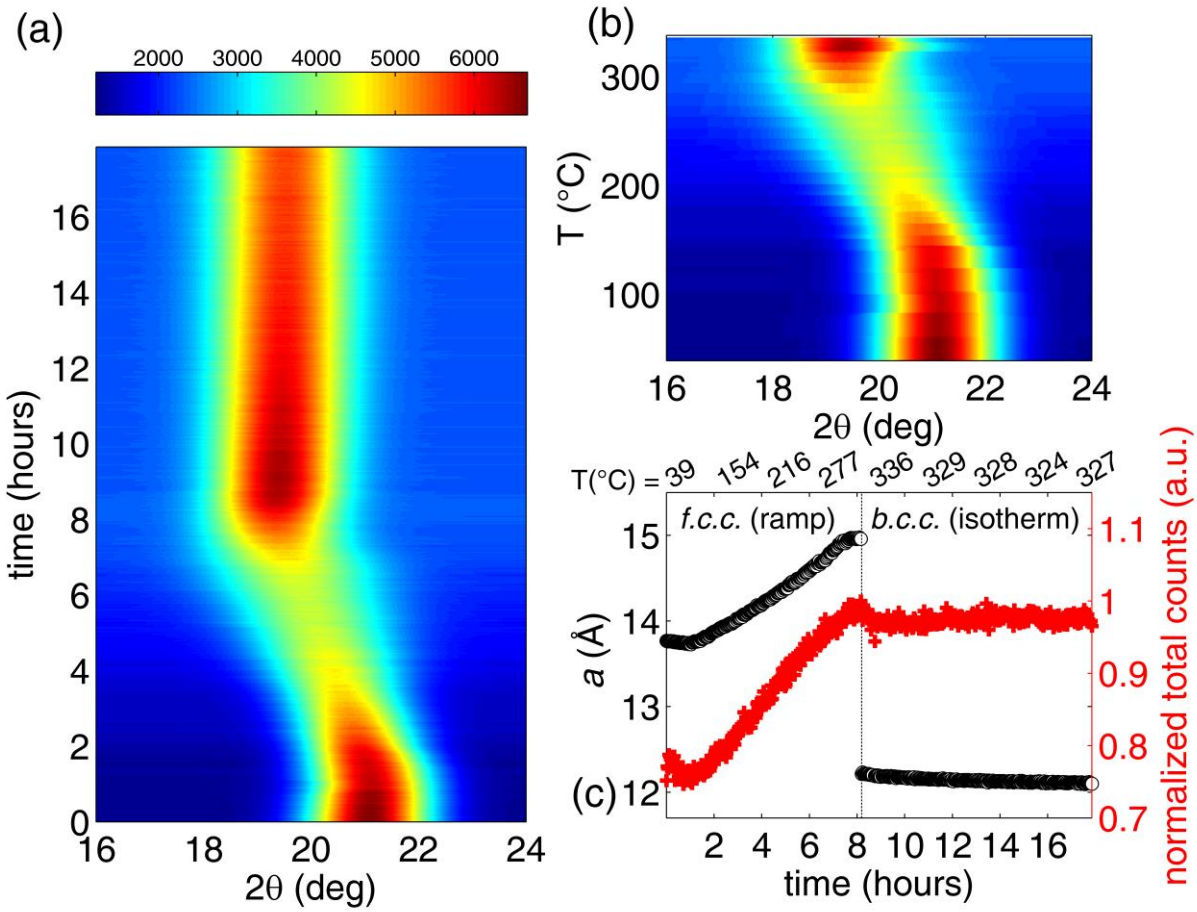

Figure 4: The Gaussian fit of the cubic Li_6C_{60} reflection in the neutron diffraction data as a function of time (a) and temperature (b) during the experiment (only the fit during the ramp is shown in b). (c) The Li_6C_{60} *fcc* and pseudo-*bcc* lattice parameter obtained from Gaussian fitting (open circles) and the total neutron intensity (crosses) as a function of time and with discrete temperature points reported.

The deuterium desorption measurement of the sample after the *in situ* experiment is displayed, as a function of time, in Figure 5. The total amount of desorbed deuterium corresponds to 3.4 wt%, equivalent to about 1.7 wt% H_2. This is in good agreement with the amount of deuterium calculated from the normalized neutron total counts.

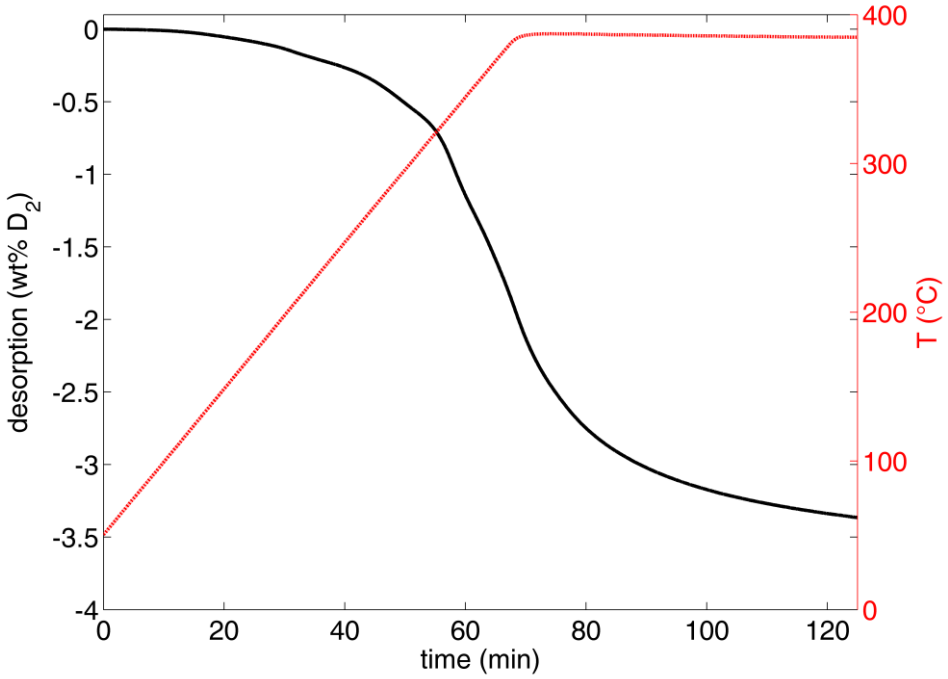

Figure 5: (a) Desorption measurement of deuterated Li_6C_{60} (390 °C, 0.5 bar H_2).

4. Discussion

The results show that the absorption of hydrogen by Li_6C_{60} is a complex process. The high (icosahedral) symmetry of C_{60} allows the description of the molecule by just three inequivalent carbon atoms in the asymmetric unit. If any of them would bind an atom of deuterium, the C_{60} deuteration would consist of only three steps, one for each inequivalent carbon. The reality is more complex: as soon as one of the inequivalent carbon atoms binds the first deuterium, the sp^2 orbital hybridization becomes sp^3 and the symmetry of the molecule is inevitably lowered. Consequently, the number of possible stages involved in the absorption increases exponentially as soon as the process starts and the number of chemisorbed hydrogens is naturally limited below 60 before the

cage collapses. Our approximation finds at least three main processes. During the first two processes, the overall symmetry remains essentially unchanged, in the first approximation, and only an expansion of the *fcc* lattice occurs.

One of the main results of this study is the evidence that the first absorption process involves only the C_{60} anions and no LiD is formed. Therefore, the presence of Li in the cell is of fundamental importance in the hydrogen-storage mechanism. Pure C_{60} starts to absorb hydrogen only at ~ 330-350 °C and 200 bar H_2 (well above the 140 °C of Li_6C_{60} deuterated at 60 bar) and with very slow kinetics.[9] The additional Li in Li_6C_{60} allows the absorption of D_2 (and H_2) to occur at much lower temperature. We can simplify this process (1) with the equation:

$$Li_6C_{60} + 4D_2 \xrightarrow{140\,^{\circ}C} Li_6C_{60}D_8(fcc) \qquad (1)$$

The number of deuterium atoms absorbed by Li_6C_{60} at this stage was approximatively calculated by considering the total neutron intensity at the end of process 1. This deuterium is likely to be chemically bound to fullerene, since the direct hydrogenation of the C_{60} anion, as a first step of hydrogen-absorption process in Li_6C_{60}, was already shown to occur by means of muon spin-relaxation spectroscopy.[6] This is, however, not a general rule in fullerides as the formation of Li-D covalent bonds was also highlighted by the same technique as a first hydrogenation step in $Li_{12}C_{60}$.[7]

The second process begins with the formation of LiD from deuterated Li_6C_{60}. Unfortunately, it is not possible to determine the amount of segregated LiD solely from powder-diffraction data, since the structure factor of hydrofulleride is unknown. However, a maximum in the normalized total counts is achieved at the end of this stage (corresponding to 1.95 wt% H_2). The following equation can describe this process:

$$Li_6C_{60}D_8(fcc) + \frac{y}{2}D_2 \xrightarrow{200\,^{\circ}C} Li_{6-\alpha}C_{60}D_{8+y-\alpha}(fcc) + \alpha LiD \qquad (2)$$

where $0 < \alpha < 6$ and represents the amount of segregated LiD. If $\alpha = 0$, no LiD is segregated and overall 15 deuterium atoms are bound to C_{60} (as calculated from the normalized total counts). Speculatively, α is likely to be greater than one since by the end of process 3 (see below) the intensity of the LiD 111 reflection has decreased by about 60%, corresponding to a non-integer stoichiometry if $\alpha = 1$. Moreover, the chemisorption of hydrogen by fullerene occurs through the saturation of the carbon sp^2 hybrid orbitals and the subsequent formation of C-H bonds. Consequently, only an even number of hydrogens can be bound to C_{60}[18] and α could be 3 or 5, leading to the formation of $Li_3C_{60}D_{12}$ or $Li_1C_{60}D_{10}$, respectively. The reasons for the origin of the formation of LiD are not evident. However, we can consider two different hypotheses. (1) The steric hindrance exerted by 10–12 hydrogens on C_{60} could not allow the stability of more than (6-α) Li ions in the *fcc* cell (*i.e.* the free volume decreases and the Li-cluster is too large to remain in the *fcc* cell). (2) The LUMOs of the $C_{60}D_{8+y-\alpha}$ molecule are able to host a lower number of electrons than C_{60} and the excess Li returns to the metallic state, permitting the formation of LiD.

The third process starts at 315 °C and continues for large part of the 330 °C hold. About 60% of the LiD reacts again and possibly re-intercalates in the form of Li^+. At the same time, a second hydrofulleride phase segregates from the former. About 0.21 wt% of H_2 equivalent is released during this process (two D atoms). This deuterium is likely to be released from LiD during the re-intercalation. Moreover, from the variation of the relative integrated intensities of the two deuterated fullerene phases (see Figure 3), it is possible to deduce that the transition from the *fcc* to the pseudo-*bcc* structures occurs between two line-phases (*i.e.* the disappearance of the *fcc* phase occurs progressively with the appearance of a new *bcc* structure that is thermodynamically more stable). We can tentatively describe this last stage of absorption by the following equation:

$$Li_{6-\alpha}C_{60}D_{8+y-\alpha}(fcc) + \alpha LiD \overset{315°C}{\longleftrightarrow} Li_{6-\alpha+2}C_{60}D_{8+y-\alpha}(bcc) + (\alpha - 2)LiD \qquad (3)$$

The fact that when the *bcc* phase increases some Li re-intercalates is not unexpected, since a *bcc* arrangement of molecules (rather than a *fcc* lattice) possesses interstitial space for more Li ions. The last step of hydrogenation is the slowest because, when LiD reacts with the hydrofulleride ($Li_{6-\alpha}C_{60}D_{8+y-\alpha}$), the limiting process is the ionic diffusion of Li^+ in the deuterated phase which is reported to be slow.[13] In order to confirm this hypothesis we fit the time evolution of the integrated intensity of the Li_6C_{60} *bcc* 311 reflection with the Johnson-Mehl-Avrami (JMA) model to understand further the nucleation and growth process:[19–21]

$$I_{311}^{bcc} = I_{311}^{bcc}(t_i)[1 - \exp(-[k(t - t_i)]^n)] \quad (4)$$

Here *k* is the kinetic constant, t_i is the time at which the phase transition starts and *n* is the JMA exponent. The fit was carried out considering only the data at constant temperature (*i.e.* during the isotherm).

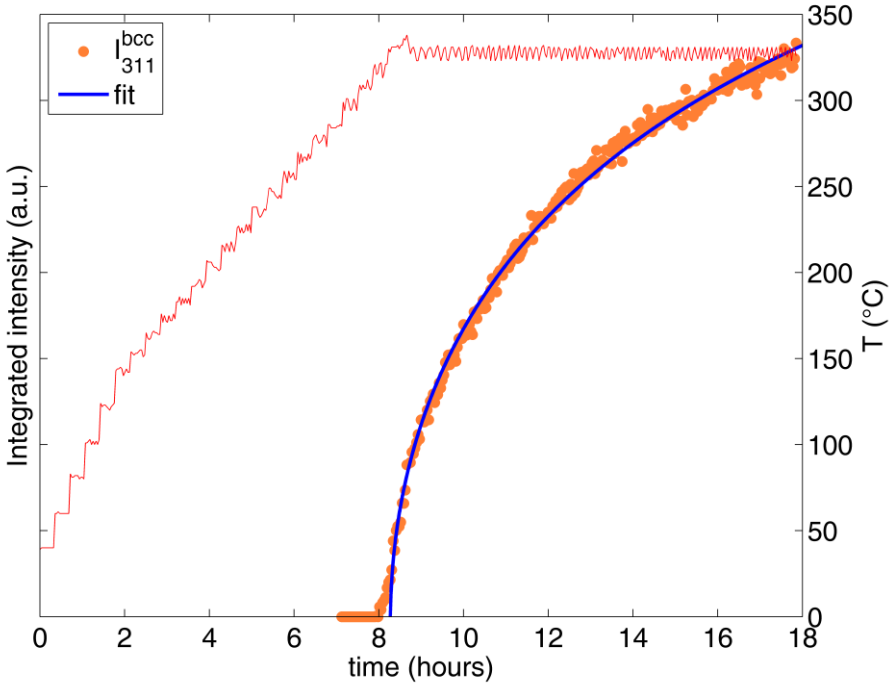

Figure 6: Integrated intensity of the 311 *bcc* reflection (left y-axis) and the fit according to the Johnson-Mehl-Avrami equation. The temperature is shown on the right y-axes.

The fit is shown in Figure 6 and yields k = 8.4(6) % h^{-1}, t_i = 8.28(1) h and n = 0.537(3). The Avrami exponent n has been considered previously for hydrogenation processes to provide information about the rate-limiting step of the reaction and is generally between 1 and 4,[22] although values lower than unity can be found in case of diffusion controlled growth.[24] For instance, for magnesium hydride formation n ~ 0.5 during the absorption process,[23] similar to what we observe for the *bcc* hydrofulleride formation. The process of magnesium hydride formation was found to be limited by the dissociation and diffusion of hydrogen in the system. A similar process happens in our system, where, instead of the hydrogen, the diffusion of Li^+ ions from the LiD decomposition into the *bcc* phase (starting at the grain's surface) is limited by the low ionic diffusion in this phase. It is also worth noting that after the segregation of Li from hydrofulleride the absorption process on C_{60} stops. This is in agreement with the hypothesis of spillover-like effect of Li clusters in Li_6C_{60}:[6] the intercalated Li clusters are effective in dissociating the hydrogen molecules and, when Li is segregated in the form of LiH (or LiD), the chemisorption process on C_{60} is not promoted anymore. At the end of the absorption process (~2 wt% H_2 at 300 °C, 60 bar D_2) the lattice volume of Li_6C_{60} increases by about 26%. Compared to the volumetric increase per wt% H_2 of Mg (~25.5% volume increase in MgH_2, corresponding to about 7.7 wt% H_2), in these conditions the Li_6C_{60} expansion is about 4 times greater if normalized to the amount of stored hydrogen. In any case, Li_6C_{60} can easily reversibly accommodate 5.9 wt% H_2 (absorption at 350 °C under 100 bar H_2 with a Pd catalyst).[2] From 2 to 5.9 wt% H_2 the lattice volume increase is very small (less than 2%) since the space occupied by a semi-hydrogenated fullerene does not differ much from that occupied by a highly hydrogenated C_{60} (such as $C_{60}H_{36}$ or $C_{60}H_{48}$). At its maximum hydrogen content, the volumetric expansion of Li_6C_{60} normalized by the wt% of stored hydrogen is just 1.5 times greater than the same value for Mg. Although molecular systems are commonly-considered less attractive than metal hydrides for applied hydrogen-storage purposes, especially because of their low density, fullerene stands out for its ability to reversibly chemisorb large quantities of hydrogen at mild conditions and with a limited volume expansion.

5. Conclusions

The deuterium absorption by Li_6C_{60} at 330 °C and 60 bar D_2 pressure was investigated using *in situ* neutron powder-diffraction. The overall absorption process can be described using three different sub-stages of reaction: (1) the first deuteration of Li_6C_{60}, occurring through an anomalous *fcc* lattice expansion and leading to the formation of $Li_6C_{60}D_8$. (2) The partial segregation of LiD and the deuteration of fullerene (up to about 2 wt% of equivalent H_2 is chemisorbed). (3) The formation of two line phases and the structural transition to a new *bcc* hydrofulleride structure. In particular, we found that the low ionic diffusion of lithium (after its partial decomposition from LiD) into the new *bcc* phase is the step limiting the kinetic of the process.

In conclusion, our neutron-diffraction study evidences the catalytic effect of Li that, together with the charged state of C_{60}, constitutes the necessary ingredient for the absorption of hydrogen in this new class of materials, allowing the absorption to take place reversibly at temperatures suitable for on board application.

6. Acknowledgments

The authors would like to acknowledge the financial support from the Cariplo foundation (Project number 2013-0592, “Carbon based nanostructures for innovative hydrogen storage systems”) and IRSES-EU Project MagNonMag nr. 295180.

References

(1) Teprovich, J. A.; Wellons, M. S.; Lascola, R.; Hwang, S.-J.; Ward, P. a; Compton, R. N.; Zidan, R. Synthesis and Characterization of a Lithium-Doped Fullerane (Lix-C60-Hy) for Reversible Hydrogen Storage. *Nano Lett.* **2012**, *12*, 582–589.

(2) Aramini, M.; Milanese, C.; Pontiroli, D.; Gaboardi, M.; Girella, A.; Bertoni, G.; Riccò, M. Addition of Transition Metals to Lithium Intercalated Fullerides Enhances Hydrogen Storage Properties. *Int. J. Hydrogen Energy* **2014**, *39*, 2124–2131.

(3) Rosseinsky, M. J.; Murphy, D. W.; Fleming, R. M.; Tycko, R.; Ramirez, A. P.; Dabbagh, G.; Barrett, S. E. Structural and Electronic Properties of Sodium-Intercalated C60. *Nature* **1992**, *356*, 416–418.

(4) Giglio, F.; Pontiroli, D.; Gaboardi, M.; Aramini, M.; Cavallari, C.; Brunelli, M.; Galinetto, P.; Milanese, C.; Riccò, M. Li12C60: A Lithium Clusters Intercalated Fulleride. *Chem. Phys. Lett.* **2014**, *609*, 155–160.

(5) Yildirim, T.; Zhou, O.; Fischer, J. E.; Bykovetz, N.; Strongin, R. A.; Cichy, M. A.; Smith III, A. B.; Lin, C. L.; Jelinek, R. Intercalation of Sodium Heteroclusters into the C60 Lattice. *Nature* **1992**, *360*, 568–571.

(6) Aramini, M.; Gaboardi, M.; Vlahopoulou, G.; Pontiroli, D.; Cavallari, C.; Milanese, C.; Riccò, M. Muon Spin Relaxation Reveals the Hydrogen Storage Mechanism in Light Alkali Metal Fullerides. *Carbon N. Y.* **2014**, *67*, 92–97.

(7) Gaboardi, M.; Cavallari, C.; Magnani, G.; Pontiroli, D.; Rols, S.; Riccò, M. Hydrogen Storage Mechanism and Lithium Dynamics in Li12C60 Investigated by μSR. *Carbon N. Y.* **2015**, *90*, 130–137.

(8) Mauron, P.; Remhof, A.; Bliersbach, A.; Borgschulte, A.; Züttel, A.; Sheptyakov, D.; Gaboardi, M.; Choucair, M.; Pontiroli, D.; Aramini, M.; et al. Reversible Hydrogen Absorption in Sodium Intercalated Fullerenes. *Int. J. Hydrogen Energy* **2012**, *37*, 14307–14314.

(9) Mauron, P.; Gaboardi, M.; Remhof, A.; Bliersbach, A.; Sheptyakov, D.; Aramini, M.; Vlahopoulou, G.; Giglio, F.; Pontiroli, D.; Riccò, M.; et al. Hydrogen Sorption in Li12C60. *J. Phys. Chem. C* **2013**, *117*, 22598–22602.

(10) Mauron, P.; Gaboardi, M.; Pontiroli, D.; Remhof, A.; Riccò, M.; Züttel, A. Hydrogen Desorption Kinetics in Metal Intercalated Fullerides. *J. Phys. Chem. C* **2015**, *119*, 1714–1719.

(11) Studer, A. J.; Hagen, M. E.; Noakes, T. J. Wombat: The High-Intensity Powder Diffractometer at the OPAL Reactor. *Phys. B Condens. Matter* **2006**, *385-386*, 1013–1015.

(12) Riccò, M.; Belli, M.; Pontiroli, D.; Mazzani, M.; Shiroka, T.; Arčon, D.; Zorko, a.; Margadonna, S.; Ruani, G. Recovering Metallicity in A4C60: The Case of Monomeric Li4C60. *Phys. Rev. B* **2007**, *75*, 081401.

(13) Maidich, L.; Pontiroli, D.; Gaboardi, M.; Lenti, S.; Magnani, G.; Riva, G.; Carretta, P.; Marini, A.; Milanese, C.; Riccò, M.; et al. Investigation of Li and H Dynamics in Li6C60 and Li6C60Hy. *unpublished* **2015**.

(14) Bürgi, H.-B.; Restori, R.; Schwarzenbach, D. Structure of C 60 : Partial Orientational Order in the Room-Temperature Modification of C 60. *Acta Crystallogr. Sect. B Struct. Sci.* **1993**, *49*, 832–838.

(15) Arvanitidis, J.; Papagelis, K.; Margadonna, S.; Prassides, K.; Fitch, A. N. Temperature-Induced Valence Transition and Associated Lattice Collapse in Samarium Fulleride. *Nature* **2003**, *425*, 599–602.

(16) Smith, D. K.; Leider, H. R. Low-Temperature Thermal Expansion of LiH, MgO and CaO. *Journal of Applied Crystallography*, 1968, *1*, 246–249.

(17) Molodets, A. M.; Lobach, A. S.; Zhukov, A. N.; Shulga, Y. M.; Fortov, V. E. Stability of Crystalline Structure and Molecules of Hydrofullerene C60H36 under High Shock Pressures. *Dokl. Phys.* **2008**, *53*, 562–565.

(18) *Fulleranes*; Cataldo, F.; Iglesias-Groth, S., Eds.; Springer, 2010; Vol. 2.

(19) Avrami, M. Kinetics of Phase Change. I General Theory. *J. Chem. Phys.* **1939**, *7*, 1103.

(20) Avrami, M. Kinetics of Phase Change. II Transformation-Time Relations for Random Distribution of Nuclei. *J. Chem. Phys.* **1940**, *8*, 212.

(21) Avrami, M. Granulation, Phase Change, and Microstructure Kinetics of Phase Change. III. *J. Chem. Phys.* **1941**, *9*, 177.

(22) Montone, a.; Aurora, A.; Mirabile Gattia, D.; Vittori Antisari, M. On the Barriers Limiting the Reaction Kinetics between Catalysed Mg and Hydrogen. *Scr. Mater.* **2010**, *63*, 456–459.

(23) Montone, A.; Aurora, A.; Gattia, D. M.; Antisari, M. V. Microstructural and Kinetic Evolution of Fe Doped MgH2 during H2 Cycling. *Catalysts* **2012**, *2*, 400–411.

(24) Christian, J. W. Ch12: Formal Theory of Transformation Kinetics. *Theory Transform. Met. Alloy.* **2002**, *529*, 529–552.